

# Molecular Geometry-aware Transformer for accurate 3D Atomic System modeling

Zheng Yuan<sup>1</sup> Yaoyun Zhang<sup>1</sup> Chuanqi Tan<sup>1</sup> Wei Wang<sup>1</sup> Fei Huang<sup>1</sup> Songfang Huang<sup>1</sup>

## Abstract

Molecular dynamic simulations are important in computational physics, chemistry, material, and biology. Machine learning-based methods have shown strong abilities in predicting molecular energy and properties and are much faster than DFT calculations. Molecular energy is at least related to atoms, bonds, bond angles, torsion angles, and nonbonding atom pairs. Previous Transformer models only use atoms as inputs which lack explicit modeling of the aforementioned factors. To alleviate this limitation, we propose **Moleformer**, a novel Transformer architecture that takes nodes (atoms) and edges (bonds and nonbonding atom pairs) as inputs and models the interactions among them using rotational and translational invariant geometry-aware spatial encoding. Proposed spatial encoding calculates relative position information including distances and angles among nodes and edges. We benchmark Moleformer on OC20 and QM9 datasets, and our model achieves state-of-the-art on the initial state to relaxed energy prediction of OC20 and is very competitive in QM9 on predicting quantum chemical properties compared to other Transformer and Graph Neural Network (GNN) methods which proves the effectiveness of the proposed geometry-aware spatial encoding in Moleformer.

## 1. Introduction

Molecular dynamic simulations (MDS) are essential in many subjects including physics, chemistry, biology, and materials (Karplus & Petsko, 1990; Van Gunsteren & Berendsen, 1990; Frenkel & Smit, 2002; Luding, 2005; Durrant & McCammon, 2011). Density function theory (DFT) is the most commonly used computational tool for simulating atomic systems and estimating the energy of molecular systems (Cohen et al., 2012). While DFT can

provide highly accurate estimations, it is extremely slow to apply to large atomic systems due to numerous iterate steps (Jones, 2015). Machine learning methods can estimate molecular system energy from *ab initio* states which do not need to inference multiple times and have satisfied performances. Machine learning methods use positional information and atomic numbers of atoms and estimate potential energy using neural networks (Schütt et al., 2018; Shi et al., 2022).

The basic form of force field for the molecular system energy can be decomposed into a sum of functions based on factors including bonds, bond angles, torsion angles, and nonbonding interactions (including electrostatic and van der Waals) (Gasteiger et al., 2020b; Leach, 2001). To include aforementioned factors for energy estimation, a neural network needs to learn interactions among atom-atom (forming bonds and nonbonding atom pairs), atom-bond (forming bond angles), and bond-bond (forming torsion angles). Previous Transformer-based models learn interactions among atom-atom in each Transformer layer (Shi et al., 2022; Liao & Smidt, 2022). Since one Transformer layer cannot model interactions of more than two atoms, high-order interactions (interactions among three or four atoms) are only modeled implicitly across Transformer layers.

To alleviate this limitation and leverage the power of Transformers, we propose Moleformer which explicitly models interactions among atoms and atom pairs in each Transformer layer. Moleformer takes atoms, bonds, and non-bonding atom pairs as inputs and applies a novel translational and rotational invariant geometry-aware spatial encoding to capture geometry relations among these inputs. The proposed spatial encoding is calculated by relative distances and angles of the atoms and atom pairs which is enough to determine the relative spatial geometry information among them. Interactions among atom-bond include the bond angle factor from the force field, and interactions among bond-bond include the torsion angle factor in the force field. DimeNet (Gasteiger et al., 2020b) had introduced directional embeddings which learn bond representation from the neighbor bonds. Compared to DimeNet, Moleformer can further learn atom pairs representation from nonadjacent atoms and atom pairs which may better model the nonbonding interactions

<sup>1</sup>Alibaba Group. Correspondence to: Songfang Huang <songfang.hsf@alibaba-inc.com>.

introduced from the force field.

We demonstrate our method on Open Catalyst 2020 (OC20) dataset (Chanussot et al., 2021) and the QM9 dataset (Ramakrishnan et al., 2014) and achieve competitive results to previous methods. Moleformer achieves state-of-the-art performance in predicting catalyst system relaxed energy from *ab initio* states using only *ab initio* states training data. We also propose a periodic boundary condition correction missed in previous machine learning methods which can improve the performances of relaxed states and energy prediction in OC20. Moleformer also performs better than recent state-of-the-art methods including SEGNN (Brandstetter et al., 2021) and EQGAT (Le et al., 2022) in QM9 quantum chemical properties predictions and shows strong abilities to predict molecular orbital energy.

## 2. Related Work

Machine learning-based MDS methods are gaining increasing attention due to their fast inference speed and good performance (Schütt et al., 2018; Zhang et al., 2020; Gasteiger et al., 2020a; Schütt et al., 2021; Shui & Karypis, 2020; Wang et al., 2022; Liu et al., 2021). Recent works in this direction can be mainly divided into two groups according to backbone neural network architectures: Graph Neural Networks (GNNs) (Gasteiger et al., 2020b; Hu et al., 2021; Gasteiger et al., 2021; Shuaibi et al., 2021; Zitnick et al., 2022) and Transformers (Fuchs et al., 2020; Ying et al., 2021; Shi et al., 2022; Liao & Smidt, 2022). GNNs construct graphs based on atom positions treating atoms as nodes and bonds as edges. Node representations are iteratively updated by messages aggregated nodes neighborhoods. However, GNNs can only interact with pre-defined neighborhoods in each layer. Compared to GNN models, Transformers can model interactions between all atom-atom pairs through the self-attention mechanism in each Transformer layer (Vaswani et al., 2017), which enables the model to learn complex relations between nonbonding atom pairs. Graphormer (Ying et al., 2021; Shi et al., 2022) takes atoms as inputs and modifies absolute positional encoding in Transformers by using the relative distance between atoms to represent geometric information. Different from Graphormer, Moleformer uses atoms and edges as inputs and uses the relative geometry information between atoms and edges.

## 3. Methods

Consider a 3D atom system with  $N$  atoms (i.e. nodes) described by nuclear charges  $\{z_1, \dots, z_N\}$ ,  $z_i \in \mathbb{Z}$  and 3D positions  $\{\mathbf{x}_1, \dots, \mathbf{x}_N\}$ ,  $\mathbf{x}_i \in \mathbb{R}^3$ . The target is to predict scalar property  $y \in \mathbb{R}$  of the system (e.g. system energy, dipole moment, and heat capacity).

### 3.1. Architecture of Moleformer

Moleformer (Figure 1 (b)) is a rotation- and translation-invariant Transformer (Vaswani et al., 2017) for 3D molecular energy and property prediction. Moleformer uses nodes (atoms) and selected edges (including bonding and nonbonding atom pairs) as inputs. If an atomic system contains  $N$  atoms, there are  $C_N^2$  possible edges. Involving all possible edges into the models is computational-heavy and may introduce uninformative edges. We choose atom pairs as edges with top- $M$  closest distances. For an atomic system like a catalyst system comprising an adsorbate and a surface (Figure 1 (a)), we prefer edges between adsorbate-adsorbate atom pairs and adsorbate-surface atom pairs rather than surface-surface atom pairs. The reason is that the edges between such atom pairs are more diverse in edge lengths and atom types and may contain more information in energy modeling. We will penalize distances in surface-surface atom pairs for edge selection.

**Input Embedding** We embed edge  $(i, j)$  by nuclear charges  $z_i, z_j$  and distances between two atoms  $\|\vec{r}_{ij}\| = \|\mathbf{x}_i - \mathbf{x}_j\|$  into  $h_{ij}^0$  using RBF (Schütt et al., 2018).

$$h_{ij}^0 = \text{RBF}(z_i, z_j, \|\vec{r}_{ij}\|) \quad (1)$$

Following Shi et al. (2022), we embed atom  $i$  into  $h_i^0$  by nuclear charges  $z_i$  and distances among all other atoms:

$$h_i^0 = \text{Embed}(z_i) + \mathbf{W}_R \sum_j (\text{RBF}(z_i, z_j, \|\vec{r}_{ij}\|)) + \mathbf{b}_R \quad (2)$$

where  $\mathbf{W}_R$  and  $\mathbf{b}_R$  are parameters of the linear layer which aligns the dimension of embedding and RBF.

**Geometry-aware Transformer Layer** We concatenate  $\{h_i^0\}_{i=1}^N$  and  $\{h_{ij}^0\}$  together as inputs and apply  $L$  layer geometry-aware Transformer block to interact nodes and edges. For  $l^{\text{th}}$  layer, the inputs are  $\{h_i^l\}_{i=1}^N$  and  $\{h_{ij}^l\}$ . Transformers in the natural language processing domain (Vaswani et al., 2017; Devlin et al., 2019) usually encode absolute position information (i.e. word order) by adding positional embedding into the input representations. For 3D atomic modeling, representations need to be rotation- and translation-invariant or equivariant, so relative position information is favored. We encode relative position information in each geometry-aware Transformer layer by adding a bias into the self-attention computation:

$$A_{ij} = \frac{(h_i^l \mathbf{W}_q)(h_j^l \mathbf{W}_k)^T}{\sqrt{d}} + b(i, j) \quad (3)$$

$$a_{ij} = \frac{\exp A_{ij}}{\sum_k \exp A_{ik}} \quad (4)$$

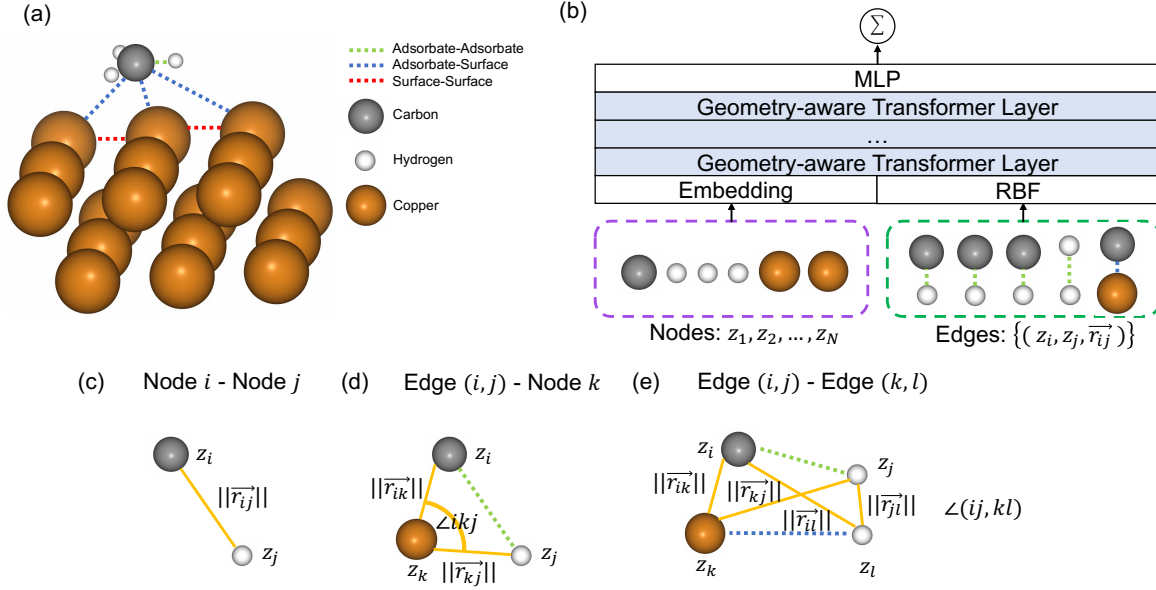


**Figure 1. The overview of Moleformer.** (a) A toy example of a catalyst system where CH<sub>3</sub> is the adsorbate and the surface is composed of copper atoms. Moleformer prefers edges between adsorbate-adsorbate atoms and adsorbate-surface atoms as model inputs. (b) Architecture of Moleformer: Nodes and selected edges are embedded by an embedding layer and an RBF layer. Stacks of geometry-aware transformer layers are used for interacting information from nodes and edges. An MLP layer is used for generating node-level or edge-level outputs, and the scalar property is predicted by summation of them. (c)-(e) show how geometry-aware spatial encoding interacts among node-node, edge-node, and edge-edge in transformer layers respectively. Dotted lines denote edges and solid yellow lines denote geometry information (i.e. distances and angles) used in the spatial encoding. (c) Distances between node-node are used. (d) Distances and angles between edge-node are used. (e) Distances and angles between edge-edge are used.

$$h_i^{l+1} = \sum_j (h_j^l \mathbf{W}_v) a_{ij} \quad (5)$$

where index  $i, j, k$  can represent a node or an edge and  $b(i, j)$  is our proposed geometry-aware spatial encoding.  $b(i, j)$  requires to capture the relative geometry information.

Specifically, if  $i$  and  $j$  are both nodes, the only relative geometry information is their distance (Figure 1 (c)), so we use RBF of distance to calculate  $b(i, j)$ :

$$b(i, j) = \text{RBF}(z_i, z_j, \|\vec{r}_{ij}\|) \quad (6)$$

An edge  $(i, j)$  and a node  $k$  form a triangle  $i, j, k$ , and the relative geometry information is determined by the lengths of two sides  $\|\vec{r}_{ik}\|, \|\vec{r}_{jk}\|$  and the included angle  $\angle ikj$  (Figure 1 (d)). We calculate bias  $b(ij, k)$  by RBF of them:

$$b(ij, k) = \text{RBF}(\|\vec{r}_{ik}\|) + \text{RBF}(\|\vec{r}_{jk}\|) + \text{RBF}(\cos \angle ikj) \quad (7)$$

Two edges  $(i, j)$  and  $(k, l)$  connecting different node pairs form a quadrilateral, and the relative geometry information is determined by lengths of six sides (i.e.  $(i, j), (i, k), (i, l), (j, k), (j, l),$  and  $(k, l)$ ). Lengths of  $(i, j)$  and  $(k, l)$  are already encoded in  $h_{ij}^l$  and  $h_{kl}^l$ . We use the

four other sides to encode  $b(ij, kl)$ . Furthermore, we enhance the spatial encoding by the angle of edges  $(i, j)$  and  $(k, l)$  to explicitly embed the angle information (Figure 1 (e)).

$$b(ij, kl) = \text{RBF}(\|\vec{r}_{ik}\|) + \text{RBF}(\|\vec{r}_{jk}\|) + \text{RBF}(\|\vec{r}_{il}\|) + \text{RBF}(\|\vec{r}_{jl}\|) + \text{RBF}(\cos(\angle ikj, \angle jkl)) \quad (8)$$

The final representations of nodes  $h_i$  and edges  $h_{ij}$  are obtained by repeatedly sending the representations into a stack of Transformer layers following the work in (Jumper et al., 2021; Shi et al., 2022). This procedure improves the model performance without enlarging parameter counts.

**Predictions** Inspired by the force field which includes bonds as factors of molecular system energy, we use not only node representations  $\{h_i\}$  but also edge representations  $\{h_{ij}\}$  for energy (and other scalar properties) predictions:

$$\hat{y} = \sum_i \text{MLP}(h_i) + \sum_{ij} \text{MLP}(h_{ij}) \quad (9)$$

where MLP is a 2-layer multi-layer perceptron with non-linearity.

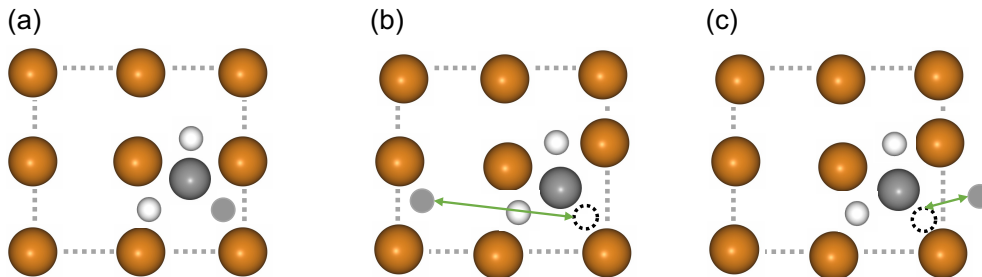


**Figure 2. PBC Correction.** (a)-(c) An example of a catalyst system where  $\text{CH}_3$  is the adsorbate and the surface is composed of copper atoms viewed along the  $\langle 110 \rangle$  orientation. The dotted lines show the borders of the unit cell. Grey-colored small atom is a hydrogen atom that goes across the unit cell and the dotted circle is its initial position. **(a)** Initial positions. **(b)** Relaxed positions. The grey hydrogen atom moves across the boundary and reappears on the opposite side. **(c)** PBC correction positions. The grey hydrogen atom lies outside the unit cell and has a smaller distance from the initial position.

### 3.2. Periodic boundary condition correction

Periodic boundary conditions (PBC) are commonly used in molecule system simulation for a large system (Makov & Payne, 1995). To implement PBC, a unit cell (which is also referred as a periodic box) is surrounded by translated copies in all directions to approximate an infinitely large system. When one molecule diffuses across the boundary of the periodic box, it reappears on the opposite side. Falling to handle such cases will cause errors in atomic distance calculation. Since distance is one of the most important input features for machine learning methods, this error is nonnegligible. For example, when considering the relative distance between an initial position  $x_i$  and a relaxed position  $x_i^r$  in a relaxation process, a long distance will be mistakenly calculated if the relaxed position appears on the opposite side of the boundary. To correctly model the local geometry, the relaxed position  $x_i^r$  is estimated by finding the smallest possible movement distance from the initial position  $x_i$ .

$$\tilde{x}_i^r = \arg \min_{x_i^r + \text{cell} * \delta} (\|x_i^r + \text{cell} * \delta - x_i\|) \quad (10)$$

where  $x_i$  is the initial position,  $\text{cell}$  are three primitive translation vectors defining the unit cell, and  $\delta = (\delta_1, \delta_2, \delta_3) \in \mathbf{R}^3$  indicates the directions of atomic movement across boundaries in which directions ( $\delta_i \in \{-1, 0, 1\}$ ). We correct the relaxed positions of atoms which do not guarantee relaxed positions are within the unit cell but preserve the correct relative position information between initial positions and relaxed positions. Figure 2 shows examples of PBC corrections of a catalyst system. In the ablation study, we will show PBC corrections improve the performances on catalyst system energy estimation.

## 4. Experiments

In this section, we show the results of Moleformer tested on the OC20 IS2RE and the QM9 datasets. Moleformer pre-

dicts molecular properties and relaxed energies accurately and outperforms prior arts.

### 4.1. Benchmarks on OC20 relaxed energy prediction

Overall, the OC20 dataset (Chanussot et al., 2021) is targeted to model the computational catalyst discovery process which is important in solar fuels synthesis, renewable fertilizer production, and energy storage (Nørskov & Bligaard, 2013; Nørskov et al., 2014; Seh et al., 2017). OC20 contains large amounts of samples in diverse adsorbates and surfaces. A large amount of training samples is suitable to test the generation ability of a machine-learning method.

Specifically, OC20 provides a small molecule called adsorbate composed of H, C, N, and O atoms, and a large surface slab composed of multiple atoms in each sample. The slab is periodic in all directions with a vacuum layer towards to adsorbate. OC20 defines three different prediction tasks: S2EF (State to energy and force), IS2RS (Initial state to relaxed state), and IS2RE (Initial state to relaxed energy). We focus our experiments on IS2RE direct setting which is the most common task in catalysis since the relaxed energy is related to catalyst properties (Chanussot et al., 2021). The direct setting is an end-to-end task that takes the initial state (i.e. atom positions) as inputs and predict the relaxed energy of systems. Relaxed energy is computed via DFT as the targets. The models need to compute the relaxed energy from the initial state directly without relaxation. Energy mean absolute error (MAE) and energy within threshold (EWT) are used as evaluation metrics. The training set contains 470K samples with 46 different adsorbates. The development set and the test sets are divided into four sub-splits including one in-domain (ID, sampled from the training distribution) split and three out-of-domain (OOD) splits, namely OOD adsorbates (unseen adsorbates), OOD catalysts (unseen element compositions for catalysts), and OOD both (both unseen adsorbate and unseen catalyst compositions). OOD adsor-

Table 1. Results on OC20 IS2RE test set using direct approach-based methods. The unit for energy MAE is meV, and the unit for Energy Within Threshold (EWT) is percentage. \* means ensembled results. ID and OOD mean in-domain and out-of-domain data split. ADS, CAT, and BOTH mean out-of-domain adsorbate, catalyst, and both (i.e. adsorbate and catalyst) data splits respectively. AVG means average results among different splits. Bolded results are the best results among non-ensembled results.

Methods	Energy MAE ↓					EWT ↑				
	ID	ADS	OOD CAT	BOTH	AVG	ID	ADS	OOD CAT	BOTH	AVG
GNS (Godwin et al., 2021)	422	568	437	465	473	<b>9.12</b>	4.25	<b>8.01</b>	4.64	<b>6.51</b>
Graphormer * (Shi et al., 2022)	398	572	417	503	472	8.97	3.45	8.18	3.79	6.10
Equiformer (Liao & Smidt, 2022)	417	548	<b>425</b>	474	466	7.71	3.70	7.15	4.07	5.66
<b>Moleformer</b>	<b>413</b>	<b>535</b>	428	<b>458</b>	<b>459</b>	8.79	<b>4.67</b>	7.58	<b>4.87</b>	6.48

bates split and OOD both split include 6 different adsorbates: CHO, CH, NH<sub>2</sub>, C<sub>2</sub>H<sub>3</sub>O<sub>2</sub>, HNO<sub>2</sub>, and C<sub>2</sub>H<sub>4</sub>(NH<sub>2</sub>)<sub>2</sub>. Each sub-split contains 25K samples. The three OOD splits serve as a good validation of the transportability and generation ability of our proposed architecture.

Notably, the training samples of OC20 are generated by the ASE tool (Atomic Simulation Environment) (Larsen et al., 2017) which uses PBC to provide atomic positions within the unit cell. As mentioned above, atomic positions at the opposite side of the unit cell need to be corrected first for an accurate geometric calculation. Therefore, the proposed PBC correction method is implemented here for data pre-processing, which has been neglected in the previous study (Shi et al., 2022). Besides, we augment the training data with noisy node data augmentation following (Godwin et al., 2021; Liao & Smidt, 2022), which first applies a linear interpolation between initial and relaxed positions and adds Gaussian noise on the interpolated positions as input. In addition to the main object of relaxed energy prediction in IS2RE, the IS2RS is used as an auxiliary node-level object to predict relaxed states (i.e., structures) (Shi et al., 2022; Liao & Smidt, 2022). Moreover, bond lengths are quadratic terms in the force field of molecular system energy. Given geometric information related to edges is used explicitly in Moleformer, we also add an edge-level object as an auxiliary loss, which needs to predict relaxed edge lengths. Contributions of PBC correction, data augmentation, and especially the auxiliary task of relaxed edge length prediction will be analyzed in the ablation study below.

We compare Moleformer with GNS (Sanchez-Gonzalez et al., 2020; Godwin et al., 2021), Graphormer (Shi et al., 2022), and Equiformer (Liao & Smidt, 2022) on IS2RE direct setting. GNS is a GNN designed for simulating complex physics with an encoder-decoder architecture. Graphormer modifies Transformer with centrality encoding, spatial encoding, and edge encoding to adapt to graph data. Equiformer is a rotational- and translational-equivariant Transformer based on irreducible representations.

Results of the test set of OC20 IS2RE are listed in Table 1

and results of the development set are listed in Appendix A. Moleformer obtains a new direct approach IS2RE state-of-the-art by achieving average energy MAE with 459 meV in the test set, which outperforms GNS with 473 meV, Graphormer with 472 meV, and Equiformer with 466 meV (with an 1.5% relative improvement). To be noticed, Moleformer outperforms the ensembled models Graphormer with a single model. For average EWT, Moleformer performs better than Graphormer and Equiformer and performs on par with GNS. For out-of-domain distribution, Moleformer achieves the lowest energy MAE and the highest EWT in OOD-ADS, and OOD-Both subsets among all methods, which shows Moleformer can better generalize to out-of-domain adsorbates.

#### 4.2. Benchmarks on QM9 properties prediction

The QM9 dataset (Ramakrishnan et al., 2014) consists of organic molecules made up of H, C, N, O, and F with 3D atom positions. The target of the QM9 dataset is to predict the energetic, electronic, and thermodynamic-related properties. Different from previous works that consider each target as single-task learning, we experiment Moleformer with a multi-task learning setting which reduces training time greatly. Gasteiger et al. (2020b) find that multi-task learning harm the performances on QM9 significantly which does not happen to Moleformer. Results compared to previous works are listed in Table 2. Some works (Schütt et al., 2018; Gasteiger et al., 2020b;a; Schütt et al., 2021; Thölke & Fabritiis, 2022) use random splits with 110K, 10K, and 10K samples in train, development, and test sets respectively. We list their results as references.

Moleformer outperforms recent state-of-the-art methods including SEGNN (Brandstetter et al., 2021) and EQGAT (Le et al., 2022) on five targets. Moleformer achieves MAE of 0.058  $a_0^3$ , 30 meV, 21 meV, 21 meV, 0.039 D, and 0.026 cal/mol K on isotropic polarizability  $\alpha$ , the gap  $\Delta\epsilon$  between  $\epsilon_{\text{HOMO}}$  and  $\epsilon_{\text{LUMO}}$ , highest occupied molecular orbital energy  $\epsilon_{\text{HOMO}}$ , lowest unoccupied molecular orbital energy  $\epsilon_{\text{LUMO}}$ , dipole moment  $\mu$ , and heat capacity at 298.15K  $C_v$

Table 2. Results on QM9 test set compared to previous works. Both random split and fix split results are reported.

Model Unit	$\alpha$ $a_0^3$	$\Delta\epsilon$ meV	$\epsilon_{\text{HOMO}}$ meV	$\epsilon_{\text{LUMO}}$ meV	$\mu$ D	$C_v$ cal/mol K
<b>Random Split</b>						
SchNet (Schütt et al., 2018)	.235	63	41	34	.033	.033
DimeNet (Gasteiger et al., 2020b)	.047	35	28	20	.029	.025
DimeNet++ (Gasteiger et al., 2020a)	.044	33	25	20	.030	.023
PaiNN (Schütt et al., 2021)	.045	46	28	20	.012	.024
ET (Thölke & Fabritiis, 2022)	.059	36	20	18	.011	.026
EQGAT (Le et al., 2022)	.053	32	20	16	.011	.024
<b>Fix Split</b>						
Cormorant (Anderson et al., 2019)	.085	61	34	38	.038	.026
SE(3)-Transformer (Fuchs et al., 2020)	.142	53	35	33	.051	.054
EGNN (Satorras et al., 2021)	.071	48	29	25	.029	.031
SEGNN (Brandstetter et al., 2021)	.060	42	24	<b>21</b>	.023	.031
EQGAT (Le et al., 2022)	.063	44	26	22	<b>.014</b>	.027
<b>Moleformer</b>	<b>.058</b>	<b>30</b>	<b>21</b>	<b>21</b>	.039	<b>.026</b>

respectively. Moleformer has significant improvement on predicting  $\Delta\epsilon$ , which is MAE of 30 meV compared to MAE of 42 meV from SEGNN. Moleformer does not achieve state-of-the-art on predicting  $\mu$ . Schütt et al. (2021) proposes a specific decoder for predicting  $\mu$ , while we only use a 2-layer MLP. The specific decoder may further enhance the performance of Moleformer. For more results on QM9 of Moleformer, we refer readers to Appendix B.

## 5. Discussion

### 5.1. Initial Structure to Relaxed Structure

To show the performance of molecular dynamic simulations, we visualize Moleformer predicted relaxed structures of catalyst systems from the OC20 dataset based on initial structures in Figure 3. Typically, relaxed structures are simulated by iteratively estimating atomic forces via DFT and updating atom positions. This may require hundred times for convergence, however, predicting relaxed structures based on initial structures only needs one step inference. From Figure 3 (a)-(c), we find that Moleformer predicts relaxed structures of in-domain adsorbates accurately. The predicted states of  $\text{C}_2\text{H}_4$  are similar to the target relaxed states, and the predicted energy is also close to the target relaxed energy. For out-of-domain adsorbates shown in Figure 3 (d)-(f), the prediction states of Moleformer are not close enough to the relaxed states and the energy difference is higher than in-domain energy estimation. We can see that Moleformer has the ability for *ab initio* relaxed state prediction, and the task of energy estimation is highly correlated to the task of state estimation.

### 5.2. Moleformer Interpretation

To understand how Moleformer models nodes and edges together, we plot the attention map for a sampled catalyst system from OC20 in Figure 4. For each input pair, we calculate the attention similarities  $A$  between them. We summarize the attention similarities in each layer and each head by counting the times that attention similarities exceed a threshold. The deep blue color indicates two inputs interact frequently, the blue color indicates two inputs interact occasionally, and the grey color indicates two inputs interact infrequently. It can be seen from Figure 4 (a) that adsorbate atoms interact with adsorbate atoms frequently, and slab atoms interact with slab atoms frequently. Adsorbate atoms interact less with slab atoms but interact more with adsorbate-related edges. This shows Moleformer uses edges to communicate the adsorbate and the slab. In Figure 4 (b), we calculate the attention similarities of the last layer from Moleformer. The Oxygen atom  $\alpha$  has the highest attention similarity to the edge A connecting the Hydrogen atom and the nearest Gallium atom. The Carbon atom  $\beta$  has the highest attention similarity to the edge B connecting the Hydrogen atom and the nearest Manganese atom. These two edges are nonbonding atom pairs which may be neglected by other machine-learning models which only consider bonded atom pairs. These attentions involve three different atoms at once, which shows that Moleformer has the ability to model complex atom interactions.

### 5.3. Ablation Study

In order to measure the contributions of PBC correction, noisy node data augmentation and an auxiliary edge-level loss, we perform ablation studies on the OC20 dataset. The experiments are conducted repeatedly, with one module removed each time. The results are listed in Table 3.

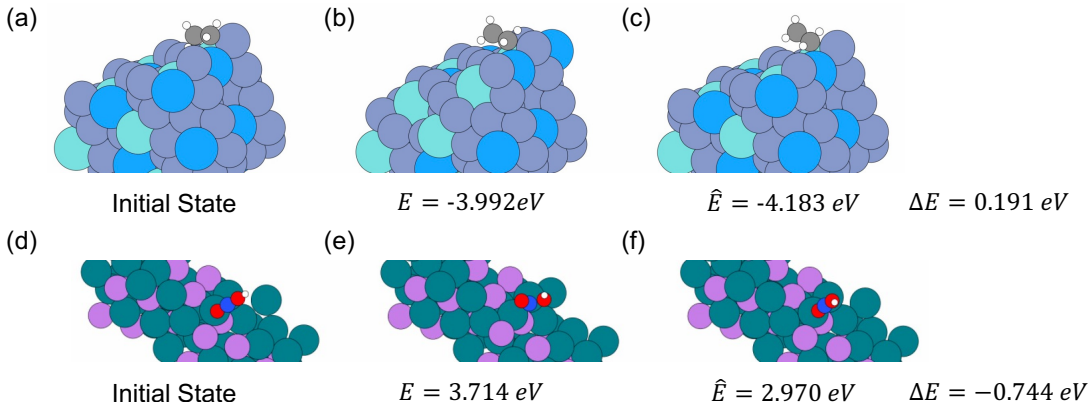


Figure 3. **IS2RS examples for Moleformer.** (a),(d) Initial states. (b),(e) Relaxed states and adsorption energies in relaxed states (i.e. targets). (c), (f) Predicted states and predicted energies from Moleformer. (a)-(c) An in-domain catalyst system with adsorbate  $C_2H_4$  and slab composed of Chromium, Zirconium, and Tantalum. (d)-(f) An out-of-domain catalyst system with adsorbate  $HNO_2$  and slab composed of Arsenic and Rhodium.

As shown in Figure 5, PBC corrections reduce the position MAE of IS2RS by calculating moving distances correctly. As a result, in in-domain split, an energy MAE improvement of 0.014 eV and an EWT improvement of 0.7% in IS2RE are obtained, validating the effectiveness of PBC corrections. From Table 3, we observe training without PBC correction, the energy MAE of the in-domain split and out-of-domain splits increase consistently.

Moreover, without noisy node augmentation, the energy MAE of the out-of-domain adsorbate split increases significantly, while the energy MAE of the out-of-domain catalyst split has a minor change. The OC20 dataset has only 82 adsorbates (this number is different from the IS2RE dataset since other adsorbates appear in the S2EF dataset) and up to  $10^5$  various catalyst slabs. Training on OC20 is easy to overfit on limited adsorbates. Noisy node augmentation provides different initial states of adsorbates and improves the generalization abilities.

Given that Moleformer introduces graph edges as inputs, and we add an auxiliary edge-level loss by predicting relaxed edge lengths. Removing edge-level auxiliary loss increases energy MAE in both in-domain split and out-of-domain splits. Previous works (Godwin et al., 2021; Shi et al., 2022; Liao & Smidt, 2022) have proven that adding node-level auxiliary loss helps energy estimation, here we find that adding edge-level auxiliary loss also works. Consider all atoms in a system as a set, the system energy is contributed by all elements in the power set (including atoms, bonds (2 atoms), angles (3 atoms), etc.). Since bond lengths are highly related to energy, introducing supervision for bonds naturally helps the estimation of energy.

Overall, adding the auxiliary edge-level loss achieved the largest performance gain among the three modules indicat-

Table 3. Ablation studies on OC20 IS2RE **development** set with energy MAE. The unit for energy MAE is meV.

Splits Settings	ID	OOD		AVG	
	ADS	CAT	BOTH		
Moleformer	<b>413</b>	<b>523</b>	432	<b>473</b>	<b>460</b>
- PBC Correction	427	551	441	495	479
- Data Augmentation	417	587	<b>429</b>	530	491
- Edge Auxiliary Loss	433	576	441	529	495

ing the effectiveness of integrating geometric information related to edges into the Moleformer architecture.

## 6. Conclusion

This work introduces Moleformer, a novel Transformer architecture to estimate 3D atomic system energy and properties. Moleformer is inspired by the force field for molecular system energy calculation which considers bonds, bond angles, torsion angles, and nonbonding interactions as factors. Moleformer leverages atoms and atom pairs as inputs, and models factors above by geometry-aware spatial encoding. We have shown that Moleformer is more accurate in predicting atomic system energy and properties than other GNN and Transformer models. GNNs have dominated the 3D atomic system modeling due to the nature of molecules which are composed of atoms (nodes) and bonds (edges). Transformers are powerful in sequential data, especially in texts, which need specific domain inductive bias to adapt to other data formats. The inductive biases in Moleformer are (1) interactions among nodes, bonds, and nonbonding atoms contribute to system energy; (2) interactions among several atoms are determined by their atomic numbers, relative distances, and angles. These inductive biases make

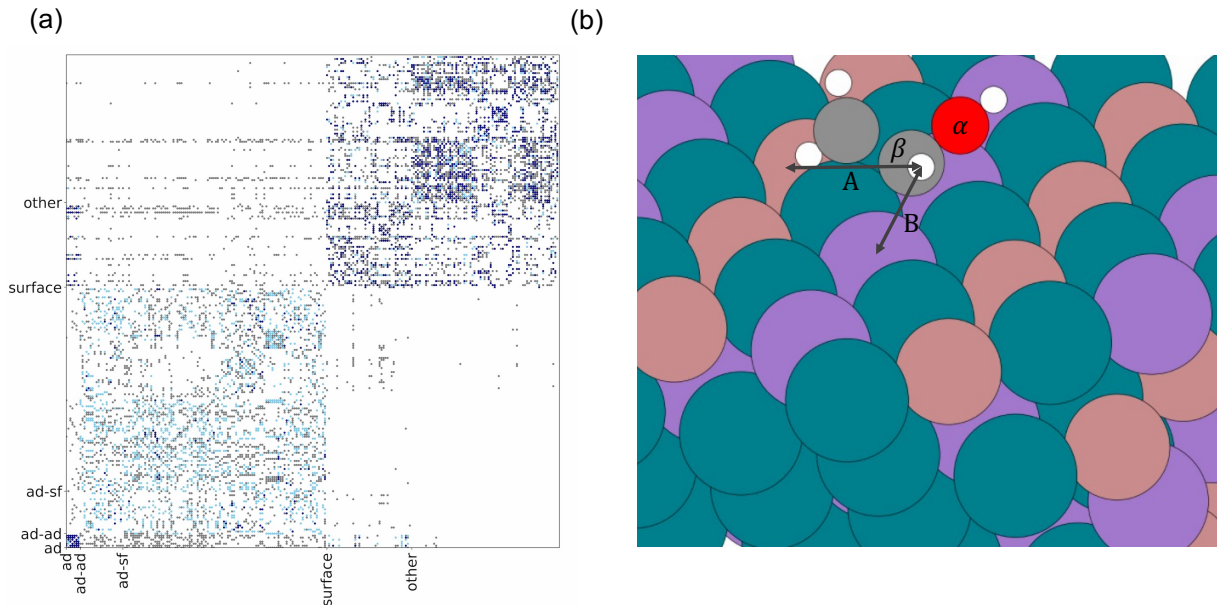


Figure 4. A catalyst system sampled from the OC20 dataset where  $\text{H}_2\text{C}=\text{CHOH}$  is the adsorbate molecule (Hydrogen atom in white, Carbon atom in grey, and Oxygen atom in red) and the slab is composed of Manganese (in purple), Rhodium (in dark green), and Gallium (in dark red) atoms. (a) The attention map calculated by Moleformer in this catalyst system. In X and Y-axes, ad means adsorbate and sf means the surface of the slab. The deeper color indicates more attention between these inputs. (b) 3D visualization of the catalyst system, two adsorbate-surface edges (A and B) have the highest attention value with an Oxygen atom  $\alpha$  and a Carbon atom  $\beta$  of the adsorbate.

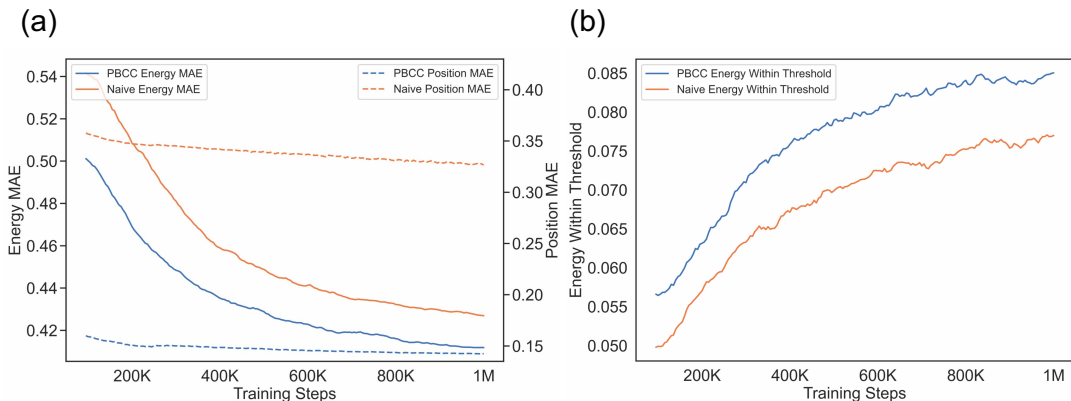


Figure 5. **Ablation study on PBC Correction.** With PBC correction, Moleformer achieves better position MAE in IS2RS and better energy MAE and EWT in IS2RE. Results of MAE and EWT are obtained in the OC20 in-domain validation set.

Moleformer suited for 3D atomic system modeling. A possible direction for future work is to introduce higher-order factors that contributed to system energy into the model.

Moleformer improves molecular energy estimation performance by involving edges and performing the attention mechanism among nodes and edges. However, this leads to more memory and computational requirements. Compared to GNNs, Transformer-based models are memory and computationally intensive. The further development direction of Moleformer can be adapting to a light-weight Transformer.

For machine learning methods, generalization ability is an important factor. Moleformer shows consistent improvement in in-domain molecular and out-of-domain molecular for energy prediction in the OC20 dataset. Moleformer improves out-of-domain molecular by extending edge features and interactions. However, energy predictions of out-of-domain molecular still have a performance gap with in-domain molecular. Another direction is to further improve the generalization ability for unseen molecules which will be useful in the design of *de novo* molecular.

## References

- Anderson, B., Hy, T. S., and Kondor, R. Cormorant: Covariant molecular neural networks. In Wallach, H., Larochelle, H., Beygelzimer, A., d'Alché-Buc, F., Fox, E., and Garnett, R. (eds.), *Advances in Neural Information Processing Systems*, volume 32. Curran Associates, Inc., 2019. URL <https://proceedings.neurips.cc/paper/2019/file/03573b32b2746e6e8ca98b9123f2249b-Paper.pdf>.
- Brandstetter, J., Hesselink, R., van der Pol, E., Bekkers, E., and Welling, M. Geometric and physical quantities improve e(3) equivariant message passing. 2021.
- Chanussot, L., Das, A., Goyal, S., Lavril, T., Shuaibi, M., Riviere, M., Tran, K., Heras-Domingo, J., Ho, C., Hu, W., Palizhati, A., Sriram, A., Wood, B., Yoon, J., Parikh, D., Zitnick, C. L., and Ulissi, Z. Open catalyst 2020 (oc20) dataset and community challenges. *ACS Catalysis*, 11(10):6059–6072, 2021. doi: 10.1021/acscatal.0c04525. URL <https://doi.org/10.1021/acscatal.0c04525>.
- Cohen, A. J., Mori-Sánchez, P., and Yang, W. Challenges for density functional theory. *Chemical reviews*, 112(1): 289–320, 2012.
- Devlin, J., Chang, M.-W., Lee, K., and Toutanova, K. BERT: Pre-training of deep bidirectional transformers for language understanding. In *Proceedings of the 2019 Conference of the North American Chapter of the Association for Computational Linguistics: Human Language Technologies, Volume 1 (Long and Short Papers)*, pp. 4171–4186, Minneapolis, Minnesota, June 2019. Association for Computational Linguistics. doi: 10.18653/v1/N19-1423. URL <https://aclanthology.org/N19-1423>.
- Durrant, J. D. and McCammon, J. A. Molecular dynamics simulations and drug discovery. *BMC biology*, 9(1):1–9, 2011.
- Frenkel, D. and Smit, B. *Understanding Molecular Simulation: From Algorithms to Applications*, volume 1 of *Computational Science Series*. Academic Press, San Diego, second edition, 2002.
- Fuchs, F., Worrall, D., Fischer, V., and Welling, M. Se(3)-transformers: 3d roto-translation equivariant attention networks. In Larochelle, H., Ranzato, M., Hadsell, R., Balcan, M., and Lin, H. (eds.), *Advances in Neural Information Processing Systems*, volume 33, pp. 1970–1981. Curran Associates, Inc., 2020. URL <https://proceedings.neurips.cc/paper/2020/file/15231a7ce4ba789d13b722cc5c955834-Paper.pdf>.
- Gasteiger, J., Giri, S., Margraf, J. T., and Günnemann, S. Fast and uncertainty-aware directional message passing for non-equilibrium molecules. In *Machine Learning for Molecules Workshop, NeurIPS*, 2020a.
- Gasteiger, J., Groß, J., and Günnemann, S. Directional message passing for molecular graphs. In *International Conference on Learning Representations (ICLR)*, 2020b.
- Gasteiger, J., Becker, F., and Günnemann, S. Gemnet: Universal directional graph neural networks for molecules. *Advances in Neural Information Processing Systems*, 34: 6790–6802, 2021.
- Godwin, J., Schaarschmidt, M., Gaunt, A., Sanchez-Gonzalez, A., Rubanova, Y., Velivcković, P., Kirkpatrick, J., and Battaglia, P. W. Simple gnn regularisation for 3d molecular property prediction and beyond. In *International Conference on Learning Representations*, 2021.
- Hu, W., Shuaibi, M., Das, A., Goyal, S., Sriram, A., Leskovec, J., Parikh, D., and Zitnick, C. L. Forcenet: A graph neural network for large-scale quantum calculations. *arXiv preprint arXiv:2103.01436*, 2021.
- Jones, R. O. Density functional theory: Its origins, rise to prominence, and future. *Reviews of Modern Physics*, 87: 897–923, 2015.
- Jumper, J. M., Evans, R., Pritzel, A., Green, T., Figurnov, M., Ronneberger, O., Tunyasuvunakool, K., Bates, R., Zidek, A., Potapenko, A., Bridgland, A., Meyer, C., Kohl, S. A. A., Ballard, A., Cowie, A., Romera-Paredes, B., Nikolov, S., Jain, R., Adler, J., Back, T., Petersen, S., Reiman, D. A., Clancy, E., Zielinski, M., Steinegger, M., Pacholska, M., Berghammer, T., Bodenstein, S., Silver, D., Vinyals, O., Senior, A. W., Kavukcuoglu, K., Kohli, P., and Hassabis, D. Highly accurate protein structure prediction with alphafold. *Nature*, 596:583 – 589, 2021.
- Karplus, M. and Petsko, G. A. Molecular dynamics simulations in biology. *Nature*, 347(6294):631–639, 1990.
- Larsen, A. H., Mortensen, J. J., Blomqvist, J., Castelli, I. E., Christensen, R., Duřak, M., Friis, J., Groves, M. N., Hammer, B., Hargus, C., et al. The atomic simulation environment—a python library for working with atoms. *Journal of Physics: Condensed Matter*, 29(27):273002, 2017.
- Le, T., Noé, F., and Clevert, D.-A. Equivariant graph attention networks for molecular property prediction. *arXiv preprint arXiv:2202.09891*, 2022.
- Leach, A. *Molecular Modelling: Principles and Applications*. Prentice Hall, 2001. ISBN 9780582382107. URL <https://books.google.com/books?id=kB7jsbV-uhkC>.

- Liao, Y. and Smidt, T. E. Equiformer: Equivariant graph attention transformer for 3d atomistic graphs. *ArXiv*, abs/2206.11990, 2022.
- Liu, Z., Lin, L., Jia, Q., Cheng, Z., Jiang, Y., Guo, Y., and Ma, J. Transferable multilevel attention neural network for accurate prediction of quantum chemistry properties via multitask learning. *Journal of Chemical Information and Modeling*, 61(3):1066–1082, 2021. doi: 10.1021/acs.jcim.0c01224. URL <https://doi.org/10.1021/acs.jcim.0c01224>. PMID: 33629839.
- Loshchilov, I. and Hutter, F. Decoupled weight decay regularization. In *7th International Conference on Learning Representations, ICLR 2019, New Orleans, LA, USA, May 6-9, 2019*, 2019.
- Luding, S. Molecular dynamics simulations of granular materials. In *The physics of granular media*, pp. 297–324. Wiley, 2005.
- Makov, G. and Payne, M. Periodic boundary conditions in ab initio calculations. *Physical Review B*, 51(7):4014, 1995.
- Nørskov, J. K. and Bligaard, T. The catalyst genome, 2013.
- Nørskov, J. K., Studt, F., Abild-Pedersen, F., and Bligaard, T. *Fundamental concepts in heterogeneous catalysis*. John Wiley & Sons, 2014.
- Paszke, A., Gross, S., Massa, F., Lerer, A., Bradbury, J., Chanan, G., Killeen, T., Lin, Z., Gimelshein, N., Antiga, L., Desmaison, A., Kopf, A., Yang, E., DeVito, Z., Raison, M., Tejani, A., Chilamkurthy, S., Steiner, B., Fang, L., Bai, J., and Chintala, S. Pytorch: An imperative style, high-performance deep learning library. In *Advances in Neural Information Processing Systems 32*, pp. 8024–8035. Curran Associates, Inc., 2019.
- Ramakrishnan, R., Dral, P. O., Rupp, M., and Von Lilienfeld, O. A. Quantum chemistry structures and properties of 134 kilo molecules. *Scientific data*, 1(1):1–7, 2014.
- Sanchez-Gonzalez, A., Godwin, J., Pfaff, T., Ying, R., Leskovec, J., and Battaglia, P. Learning to simulate complex physics with graph networks. In III, H. D. and Singh, A. (eds.), *Proceedings of the 37th International Conference on Machine Learning*, volume 119 of *Proceedings of Machine Learning Research*, pp. 8459–8468. PMLR, 13–18 Jul 2020. URL <https://proceedings.mlr.press/v119/sanchez-gonzalez20a.html>.
- Satorras, V. G., Hoogeboom, E., and Welling, M. E(n) equivariant graph neural networks. In *International Conference on Machine Learning*, 2021.
- Schütt, K. T., Unke, O. T., and Gastegger, M. Equivariant message passing for the prediction of tensorial properties and molecular spectra. In *International Conference on Machine Learning*, 2021.
- Schütt, K. T., Sauceda, H. E., Kindermans, P.-J., Tkatchenko, A., and Müller, K.-R. Schnet – a deep learning architecture for molecules and materials. *The Journal of Chemical Physics*, 148(24):241722, 2018. doi: 10.1063/1.5019779. URL <https://doi.org/10.1063/1.5019779>.
- Seh, Z. W., Kibsgaard, J., Dickens, C. F., Chorkendorff, I., Nørskov, J. K., and Jaramillo, T. F. Combining theory and experiment in electrocatalysis: Insights into materials design. *Science*, 355(6321):eaad4998, 2017. doi: 10.1126/science.aad4998. URL <https://www.science.org/doi/abs/10.1126/science.aad4998>.
- Shazeer, N. Glu variants improve transformer. *arXiv preprint arXiv:2002.05202*, 2020.
- Shi, Y., Zheng, S., Ke, G., Shen, Y., You, J., He, J., Luo, S., Liu, C., He, D., and Liu, T.-Y. Benchmarking graphormer on large-scale molecular modeling datasets. *arXiv preprint arXiv:2203.04810*, 2022. URL <https://arxiv.org/abs/2203.04810>.
- Shuaibi, M., Kolluru, A., Das, A., Grover, A., Sriram, A., Ulissi, Z., and Zitnick, C. L. Rotation invariant graph neural networks using spin convolutions. *arXiv preprint arXiv:2106.09575*, 2021.
- Shui, Z. and Karypis, G. Heterogeneous molecular graph neural networks for predicting molecule properties. In *2020 IEEE International Conference on Data Mining (ICDM)*, pp. 492–500, Los Alamitos, CA, USA, nov 2020. IEEE Computer Society. doi: 10.1109/ICDM50108.2020.00058. URL <https://doi.ieeecomputersociety.org/10.1109/ICDM50108.2020.00058>.
- Thölke, P. and Fabritius, G. D. Equivariant transformers for neural network based molecular potentials. In *International Conference on Learning Representations*, 2022. URL <https://openreview.net/forum?id=zNHqzQZ9wrRB>.
- Van Gunsteren, W. F. and Berendsen, H. J. Computer simulation of molecular dynamics: methodology, applications, and perspectives in chemistry. *Angewandte Chemie International Edition in English*, 29(9):992–1023, 1990.
- Vaswani, A., Shazeer, N., Parmar, N., Uszkoreit, J., Jones, L., Gomez, A. N., Kaiser, Ł., and Polosukhin, I. Attention is all you need. *Advances in neural information processing systems*, 30, 2017.

- Wang, Z., Wang, C., Zhao, S., Xu, Y., Hao, S., Hsieh, C. Y., Gu, B.-L., and Duan, W. Heterogeneous relational message passing networks for molecular dynamics simulations. *npj Computational Materials*, 8(1):1–9, 2022.
- Ying, C., Cai, T., Luo, S., Zheng, S., Ke, G., He, D., Shen, Y., and Liu, T.-Y. Do transformers really perform bad for graph representation? In *NeurIPS*, 2021.
- Zhang, B. and Sennrich, R. Root mean square layer normalization. *Advances in Neural Information Processing Systems*, 32, 2019.
- Zhang, S., Liu, Y., and Xie, L. Molecular mechanics-driven graph neural network with multiplex graph for molecular structures. In *NeurIPS-W*, 2020.
- Zitnick, C. L., Das, A., Kolluru, A., Lan, J., Shuaibi, M., Sriram, A., Ulissi, Z., and Wood, B. Spherical channels for modeling atomic interactions. *arXiv preprint arXiv:2206.14331*, 2022.

## A. Training Details

The proof of rotational and translational invariance for Moleformer is naive since all positional features (i.e. atom pair lengths and angle among vectors) used in Moleformer are rotational and translational invariant.

**Architecture Details** We apply the layer normalization and the feed-forward network after the multi-head attention in each Transformer layer. We adopt root mean square (RMS) layer normalization (Zhang & Sennrich, 2019) following Liao & Smidt (2022). We use GEGLU (Shazeer, 2020) as the activation function in the feed-forward network.

**OC20** For training on the OC20 IS2RE dataset, we applied noisy nodes data augmentation following (Godwin et al., 2021) which augment the initial positions by linear interpolation between the initial positions and relaxed positions and add Gaussian noises  $N(0, \sigma^2)$  to adsorbate atoms and surface atoms of the slab where  $\sigma = 0.3\text{\AA}$ .

For edges used as inputs, we calculated distances between all node pairs. In the OC20 dataset, adsorbate molecules have few atoms while slabs have more atoms. If we use all node pairs as inputs, edges will be dominated by two atoms from slabs. Interactions among slab atoms are monotone, and involving too many edges from two slab atoms is not informative. We group nodes (i.e. atoms) into three groups: adsorbate atoms, surface atoms of the slab, and other atoms of the slab. Since we wanted to pay more attention to adsorbates and interactions among adsorbates and surface atoms of slabs, we group all node pairs into six groups based on node types: adsorbate-adsorbate, adsorbate-surface, surface-surface, adsorbate-other, surface-other, and other-other. We sorted all node pairs based on group types and distances and selected the top  $M$  node pairs as edges. We heuristically selected  $M$  equal to the node count, which will ignore some other-other edges which are not informative. Attention mechanism in Transformers models have  $O(N^2)$  time complexity, adding  $M = N$  edges into inputs will not change the order of time complexity.

The models were trained with IS2RE loss (system level), IS2RS auxiliary loss (node level), and relaxed edge length prediction auxiliary loss (edge level). These losses are calculated using MAE and weighted summed as the total loss:

$$\mathcal{L} = \lambda_S |\hat{E} - E| + \frac{\lambda_N}{3N} \sum_{i=1}^N \sum_{\alpha=1}^3 |\hat{x}_{i,\alpha}^r - x_{i,\alpha}^r| + \frac{\lambda_E}{M} \sum_{e=1}^M |\hat{l}_e - l_e| \quad (11)$$

where  $N$  and  $M$  are node count and edge count,  $E$  is the relaxed system energy,  $x_{i,\alpha}^r$  is the relaxed position of  $i^{th}$  atom on direction  $\alpha$ ,  $l_e$  is the relaxed length of  $e^{th}$  edge,  $\hat{\cdot}$  is the prediction from the model, and  $\lambda_S$ ,  $\lambda_N$ , and  $\lambda_E$  are weights of system, node, and edge level loss respectively. For training IS2RS auxiliary task, the model needs to predict the moving position of each atom  $\Delta \mathbf{x}_i = \mathbf{x}_i^r - \mathbf{x}_i \in \mathbb{R}^3$ , where  $\mathbf{x}_i^r$  is the relaxed position. We apply a rotational equivariant attention layer from (Shi et al., 2022) to predict  $\Delta \mathbf{x}_i$  which multiplies unit relative position  $[\frac{\vec{r}_{ij}}{\|\vec{r}_{ij}\|}]_{i,j}$  by standard multi-head attention probabilities. For the relaxed edge length prediction auxiliary task, we use a 2-layer MLP on  $h_{ij}$  to regress the relaxed edge length  $l$ . The prediction targets of  $E$  and  $x_{i,\alpha}^r$  had been normalized to zero mean and unit variance.  $\lambda_S$  was set to 1. The weights of auxiliary losses  $\lambda_N$  and  $\lambda_E$  were set to 15 and 5 at the beginning of the training and linearly decayed to 1 within the first quarter of training and remained at 1.

**QM9** For the QM9 dataset, we use the split from (Anderson et al., 2019) which contain 100K, 18K, and 13K samples in train, development, and test sets respectively.

For edges used as inputs, we select the top  $M = N$  nearest node pairs as input edges. We apply multi-task training on all 12 targets of QM9, and the total losses are calculated by summing of Smooth L1 Loss for each target. Smooth L1 Loss performs better than MSE and MAE Loss during our preliminary experiments. We first apply a linear regression with nuclear charges and targets on the training set, and the coefficients of the linear regression are used as atom references. For training Moleformer, we subtracted atom references for each target and normalize each target to zero mean and unit variance. Subtracting atom references significantly reduces the target variances and helps models converge quickly.

**Optimization** All models are implemented in PyTorch (Paszke et al., 2019) and trained with 8 NVIDIA A100 GPUs. We use AdamW (Loshchilov & Hutter, 2019) to optimize models with a linear learning rate warmup and decay. We evaluate the model at the end of training.

## B. Results of development set in the OC20 dataset

We display the results of the development set of OC20 IS2RE in Table 4. To be noticed, Equiformer with noisy nodes data augmentation seems overfitted on the development set which has a much larger difference between the development set and the test set energy MAE than other methods.

## C. Results of remaining targets in the QM9 dataset

We display the results of six other targets in Table 5. Moleformer achieves five of six targets’ best results among the fix split setting. Moleformer does not perform well in predicting  $\langle R^2 \rangle$  which may be improved via using a specialized decoder introduced by PaiNN (Schütt et al., 2021).

## D. Hyper-parameters for training Moleformer

We display the used hyper-parameters for training Moleformer in Table 6.

Table 4. Results on OC20 IS2RE development set using direct approach-based methods. The unit for energy MAE is meV, and the unit for Energy Within the Threshold (EWT) is percentage. † indicates using noisy nodes data augmentation. ID and OOD mean in-domain and out-of-domain data split. ADS, CAT, and BOTH mean out-of-domain adsorbate, catalyst, and both data splits. AVG means average results among different splits.

Methods	ID	Energy MAE ↓			AVG	ID	EWT ↑			AVG
		ADS	OOD CAT	BOTH			ADS	OOD CAT	BOTH	
GNS (Godwin et al., 2021)	540	650	550	590	583	-	-	-	-	-
GNS †	470	510	480	460	480	-	-	-	-	-
Graphormer (Shi et al., 2022)	433	585	444	530	498	-	-	-	-	-
Equiformer (Liao & Smidt, 2022)	422	542	423	475	466	7.23	3.77	7.13	4.10	5.56
Equiformer †	416	<b>498</b>	<b>417</b>	<b>434</b>	<b>441</b>	7.47	<b>4.64</b>	7.19	<b>4.84</b>	<b>6.04</b>
<b>Moleformer †</b>	<b>413</b>	523	432	473	460	<b>8.01</b>	3.04	<b>7.66</b>	3.19	5.48

Table 5. Results on remaining targets of QM9 test set compared to previous works.

Model	$U_0$	$U$	$H$	$G$	$\langle R^2 \rangle$	ZPVE
Unit	meV	meV	meV	meV	$a_0^2$	meV
<b>Random Split</b>						
SchNet (Schütt et al., 2018)	14	19	14	14	.073	1.7
DimeNet (Gasteiger et al., 2020b)	8	8	8	9	.331	1.3
DimeNet++ (Gasteiger et al., 2020a)	6	6	7	9	.331	1.2
PaiNN (Schütt et al., 2021)	6	6	6	7	.066	1.3
ET (Thölke & Fabritiis, 2022)	6	6	6	8	.033	1.8
EQGAT (Le et al., 2022)	25	25	24	23	.382	2.0
<b>Fix Split</b>						
Cormorant (Anderson et al., 2019)	22	21	21	20	.961	2.0
EGNN (Satorras et al., 2021)	12	12	12	12	.106	1.6
SEGNN (Brandstetter et al., 2021)	15	13	16	15	.660	1.6
EQGAT (Le et al., 2022)	13	13	13	12	.257	1.5
<b>Moleformer</b>	<b>10</b>	<b>10</b>	<b>12</b>	<b>11</b>	1.848	<b>1.2</b>

*Table 6.* Hyper-parameters used for training Moleformer on the OC20 dataset and the QM9 dataset.

Parameters	OC20	QM9
Embedding Dimension	768	768
Feed-forward Network Dimension	768	768
RBF Dimension	128	128
Attention Heads	48	48
Transformer Layers	12	6
Repeat Count	4	4
Epochs	70	800
Warmup Steps	10,000	1,000
Peak Learning Rate	2e-4	5e-4
Batch Size	32	256
Adam $\epsilon$	1e-6	1e-6
Weight Decay	1e-3	1e-3
Clipping Gradient	5	5